INSTITUTE OF PLASMA PHYSICS

NAGOYA UNIVERSITY

Heat Transport due to the Collisionless Tearing Instabilities

I. Katanuma

(Received - Apr.15, 1980)

IPPJ-461 May 1980

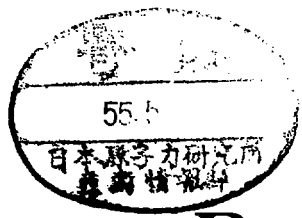

RESEARCH REPORT

NAGOYA, JAPAN

Heat Transport due to the Collisionless Tearing Instabilities

I. Katanuma

(Received - Apr.15, 1980)

IPPJ-461 May 1980

Further communication about this report is to be sent to the Research Information Center, Institute of Plasma Physics, Nagoya University, Nagoya Japan

Abstract

Collisionless tearing instabilities and the associated electron heat transport are investigated by using a two-and-one-half dimensional particle simulation code. It is shown that a collisionless drift tearing instability saturates at a low amplitude and turns into a nonlinear pure tearing instability. The electron internal energy profile is flattened within the magnetic island. The electron heat conductivity obtained from the heat flow across the singular surface is proportional to W^4 in the linear phase and to $(dW/dt)W^2$ in the nonlinear phase of the tearing instability. Here W is the half width of the magnetic island. A theoretical model to explain these results is also presented.

1. Introduction

Anomalous electron heat transport associated with magnetic perturbations, even when their amplitudes are small, have been disclosed by the experiments on tokamaks[1]. The observed flattening of the electron temperature profile around a rational magnetic surface suggests large electron heat flux across it. Tearing instabilities are thought to be one of the most probable mechanisms causing anomalous heat transport in tokamaks at such surfaces.

The electron heat transport caused by tearing instabilities in the MHD regime has been studied by Hazeltine and Strauss.[2] Their basic idea is that a small magnetic perturbation allows the parallel heat transport to contribute to the heat transport in the radial direction. If any small magnetic perturbation which connects two neighbouring magnetic surfaces is present, then there will be a consequent large heat exchange between these equilibrium magnetic surfaces. This kind of phenomena will be observed when magnetic islands are formed due to tearing instabilities or when magnetic fields are braided.[3),4)]

In view of high temperature existing in current tokamak experiments, collisionless tearing instabilities are important. Although tearing instabilities in the collisionless region have been studied extensively,[5)-9)] no reliable quantitative estimation for the associated electron heat transport is avaliable.

The purpose of this paper is to present a simulation study on collisionless tearing instabilities and the

consequent electron heat transport, using two-and-one-half dimensional magneto-static particle simulation code.

It is shown that the induced drift tearing instability saturates at a low amplitude and then turns into a nonlinear pure tearing instability. The observed electron heat conductivity increases in the linear phase in proportion to w^4 where w is a typical half width of the formed magnetic island, and continue to increase as $(dW/dt)W^2$ during the nonlinear phase.

In Sec.2, a theoretical model is presented to aid in understanding the simulation results. Quasi-linear and nonlinear treatments are worked out in a heuristic way. In Sec.3, the simulation model and the simulation results are presented and discussed in the light of the theoretical model of Sec.2. A discussions of the results and the conclusions of this work are given in Sec.4.

2. Theoretical Model

We here present a theoretical model for the electron heat transport caused by tearing instabilities. Our arguments are based on a plasma slab with a sheared magnetic field,

$$\underset{\sim}{B} = B_z\hat{e}_z + B_y(x)\hat{e}_y, \qquad |B_z| >> |B_y| , \qquad (1)$$

where the shear field $B_y(x)$ is produced by a sheet current as shown in Fig.1. The electron temperature $T_e(x)$ and the current density $J_0"(x)$ are assumed to vary only in the x direction, and the electron density is taken uniform. Namely the electron distribution in equilibrium is expressed as,

$$f_0 = \left(\frac{m_e}{2\pi T_e(x)}\right)^{3/2} \exp\left[-\frac{m_e}{2T_e(x)}(\underset{\sim}{v}-v_{0\parallel}(x)\hat{e}_z)^2\right]. \quad (2)$$

We are mainly interested in the electron dynamics under the condition of $\beta > m_e/m_i$,[8] and consider the perturbed electric and magnetic fields in the form,

$$\tilde{\underset{\sim}{B}} = \nabla \times \tilde{A}_\parallel \hat{e}_z \ , \text{ and } \tilde{E}_\parallel \hat{e}_z = -\frac{1}{c}\frac{\partial}{\partial t}\tilde{A}_\parallel \quad (3)$$

The scalar potential may be neglected for the present qualitative discussions.[5] The vector potential $\tilde{A}_\parallel$ is determined by Ampere's law,

$$\Delta\tilde{A}_\parallel = -\frac{4\pi n_0 e}{c}\int d\underset{\sim}{v} v_\parallel \tilde{f}, \quad (4)$$

in which $\tilde{f}$ is the perturbed electron distribution which obeys the linearized Vlasov equation in the small Larmor radius limit,

$$\left(\frac{\partial}{\partial t} + v_\parallel \frac{B_y}{B}\frac{\partial}{\partial y}\right)\tilde{f} = -v_\parallel \frac{\tilde{B}_x}{B}\frac{\partial}{\partial x}f_0 + \frac{e}{m_e}\tilde{E}_\parallel \frac{\partial}{\partial v_\parallel}f_0 \ . \quad (5)$$

We seek a solution of the form $\tilde{A}_\parallel(\underset{\sim}{r}, t) = \tilde{A}_\parallel(x)\exp(ik_y y - i\omega t)$. Solving Eq.(5) for $\tilde{f}$ and substituting it into Eq.(4), we obtain the eigen-mode equation as follows.

$$\left(\frac{\partial^2}{\partial x^2} - k_y^2\right)\tilde{A}_{\parallel} = \frac{1}{c^2\lambda_D^2} v_e \frac{\omega^*_{Te}}{2k_{\parallel}} \left[-s_z+\zeta_k^2 Z(\zeta)+\zeta_K^2 \zeta Z'(\zeta)\right]\tilde{A}_{\parallel}$$

$$- \frac{1}{c^2\lambda_D^2} v_e \frac{\omega}{2k_{\parallel}} \zeta_k Z'(\zeta)\tilde{A}_{\parallel}$$

$$- \frac{v_e^3 k_y}{2c^2\lambda_D^2\omega_{ce}k_{\parallel}} \left[1-\zeta_k^2 z'(\zeta)\right] \frac{\partial s_z}{\partial x} \tilde{A}_{\parallel} \quad , (6)$$

where $Z(\zeta)$ is the plasma dispersion function,[10] $Z'(\zeta) = dZ/d\zeta$, and the other symbols are ; $\zeta = (\omega/k_{\parallel}-v_{0\parallel})/v_e$, $\zeta_k = \omega/k_{\parallel}v_e$, $v_e = (2T_e/m_e)^{1/2}$, $s_z = v_{0\parallel}/v_e$, $\omega^*_{Te} = -(c/eB)dT_e(x)/dx$, $\omega_{ce} = eB/m_e c$, and $\lambda_D = (T_e/4\pi n_0 e^2)^{1/2}$. Equation (6) can be solved by a shooting method under the boundary condition that $\tilde{A}_{\parallel}=0$ at $x=0$ and $x=L_x$. Note that in our model the plasma slab is bounded by the conducting walls located at $x=0$ and $x=L_x$ as shown in Fig.1.

Suppose that a singular surface ($k_{\parallel}=0$) exists inside the plasma slab. We divide it into the inner region including the singular surface and the outer region. The width of the inner region is characterized by two parameters; the tearing mode width λ_w and the current channel width λ_σ.[8] The former is defined as the extent of the region inside which $\tilde{E}_{\parallel}\neq 0$, and is given be $\lambda_w=|\omega/k_{\parallel}'v_A|$, where v_A is the Alfven velocity and $k_{\parallel}'=dk_{\parallel}/dx$. On the other hand λ_σ is defined as the spatial region in which electrons can continuously accerelated by the parallel pertubation,

$\lambda_\sigma = |\omega/k_\parallel' v_e|$. Note that $\lambda_\sigma < \lambda_w$ for $\beta > m_e/m_i$ because that $\lambda_\sigma/\lambda_w = (m_e/m_i\beta)^{1/2}$. In the inner region, kinetic effects (electron inertia) are important. On the right side of Eq.(6), the first two terms which express kinetic effects are important in the inner region, while the last term is dominant in the outer region.

Figure 3(a) shows the dispersion relation obtained by solving Eq.(6) by a shooting method. The physical parameters used here are $c/v_e=3.53$, $\omega_{ce}/\omega_{pe}=1.5$, $L_x=64$, $k_y=\pi/32$, and $\lambda_D=1.4$. The current and temperature profiles are $J_\parallel(x) = -en_0 v_d \exp[-(\ln 2)(x-L_x/2)/25]$, and $T_e(x)=1-0.5T_s\tanh[5(x-L_x/2)/64]$ with $T_s=1.2$. As is seen in Fig.3(a), the frequency is not so dependent on v_d, which is about $0.2\omega_{Te}^*$, while the growth rate depends on v_d. A remarkable feature is that a boundary of the stability exists at finite v_d ($\neq 0$). For the case of uniform temperature ($T_s = 0$), it is shown numerically that the boundary of stability lies at the point $v_d = 0$. Then the temperature gradient has a tendency to stabilize the tearing instability.

In the following analysis we consider the case, in which $|\tilde{B}_x(k_y)|$ is constant in the inner region.

2-1. Electron Heat Conductivity in the Linear Phase

In the inner region, the magnetic shear in the y direction is small, and a magnetic island will easily be formed, when the small perturbed magnetic field $\tilde{B}_x$ is

induced. The electrons inside the magnetic island execute a bounce motion along the magnetic field lines. They, however, do not go around the island within one growth time, because the island bounce frequency is smaller than the linear growth rate. We then calculate the electron heat flux in the x direction along $\tilde{B}_x$ by invoking the quasi-linear equation,

$$\frac{\partial f_0}{\partial t} = \sum_{k_y} \left[\frac{e}{m_e} \tilde{E}_{\parallel}^{*}(k_y) \frac{\partial}{\partial v_{\parallel}} - v_{\parallel} \frac{\tilde{B}_x^{*}(k_y)}{B} \frac{\partial}{\partial x} \right] \tilde{f}(k_y), \qquad (7)$$

where superscript * represnts the complex conjugate. We introduce the effective temperature $T_e(x)$ which is defined as $T_e = \int d\underset{\sim}{v}(\underset{\sim}{v}-\bar{\underset{\sim}{v}})^2 f_0$ with $\bar{\underset{\sim}{v}} = \int d\underset{\sim}{v}\underset{\sim}{v} f_0$. Taking the appropriate moment of Eq.(7), we find the heat transport equation becomes

$$\frac{\partial}{\partial t} nT_e + F\frac{\partial T_e}{\partial x} = \frac{\partial}{\partial x} \kappa \frac{\partial}{\partial x} T_e + Q, \qquad (8)$$

where with $\zeta = \omega/k_{\parallel}v_e$,

$$\kappa = -i\sum_{k_y} \left\{ \frac{2nc}{3B^2} \tilde{B}_x^{*}(k_y)\tilde{E}_{\parallel}(k_y)\frac{k_y}{k_{\parallel}^2} \left[1 + \zeta^2+\zeta^4+(\zeta^5+ \frac{1}{2}\zeta^3 Z(\zeta)) \right] \right\}, \qquad (9)$$

$$F = -i\sum_{k_y} \left\{ \frac{2nec}{3T_e B} \tilde{E}_{\parallel}^{*}(k_y)\tilde{E}_{\parallel}(k_y)\frac{k_y}{k_{\parallel}^2} \left[\zeta^2+ (\zeta^3- \frac{1}{2}\zeta) Z(\zeta) \right] \right\}, \qquad (10)$$

$$Q = -i\sum_{k_y} \left[\frac{2ne^2}{3T_e} v_e \tilde{E}_{\parallel}^{*}(k_y)\tilde{E}_{\parallel}(k_y)\frac{1}{k_{\parallel}}(\zeta+\zeta^2 Z(\zeta)) \right]$$

$$+i\sum_{k_y}\left\{\frac{2ne\tilde{B}_x^*(k_y)}{3B}\frac{\partial}{\partial x}\left[v_e\tilde{E}_{\parallel}(k_y)\frac{1}{k_{\parallel}}\left(\frac{3}{2}\zeta+\zeta^3+\left(\zeta^2+\zeta^4\right)Z(\zeta)\right)\right]\right\} . \tag{11}$$

In the above we have assumed $v_{0\parallel} \ll v_e$. As mentioned early in this section, the boundary of the inner region is given by $|\zeta|=1$. For estimation of κ, F, and Q, we use the approximate expansion in $|\zeta|$ of $Z(\zeta)$ in the outer region where $|\zeta|<1$, and the asymptotic expansion in the inner region where $|\zeta|>1$. We find the main contribution to them comes from the inner region. Keeping only leading term, we obtain

$$\kappa \simeq \sum_{k_y}\left(\frac{3}{2}nv_e^2\frac{\tilde{B}_x^*(k_y)\tilde{B}_x(k_y)}{B^2}\frac{\gamma_k}{\omega_k^2+\gamma_k^2}\right) , \tag{12}$$

$$F \simeq \sum_{k_y}\left(\frac{4n\omega_{ce}}{3k_y}\frac{\tilde{B}_x^*(k_y)\tilde{B}_x(k_y)}{B^2}\frac{\gamma_k\omega_k}{\omega_k^2+\gamma_k^2}\right) , \tag{13}$$

$$Q \simeq \sum_{k_y}\left(\frac{2}{3}m_e n\omega_{ce}^2\frac{\tilde{B}_x^*(k_y)\tilde{B}_x(k_y)}{B^2}\frac{\gamma_k}{k_y^2}\right) . \tag{14}$$

Where ω_k and γ_k are the linear eigen-frequency and growth rate of the mode k_y. If we divide T_e into $T_{e\perp}$ and $T_{e\parallel}$, we obtain the heat transport equations for $T_{e\perp}$ and $T_{e\parallel}$. Here $T_{e\perp}$ and $T_{e\parallel}$ are the components parallel and perpendicular to the magnetic field lines, respectively. In this case the heat conductivity $\kappa^{(\parallel)}$ for $nT_{e\parallel}$ and $\kappa^{(\perp)}$ for $nT_{e\perp}$ have the following relation in the inner region,

$$\kappa \simeq \frac{1}{2}\kappa^{(\parallel)} \simeq 2\kappa^{(\perp)} \tag{15}$$

In the system in which only one mode of k_y is unstable, the relation $W \propto |\tilde{B}_x(k_y)|^{1/2}$ holds.[6] Then the electron heat conductivity κ grows in proportion to $\gamma_k W^4/(\omega_k^2+\gamma_k^2)$ in the linear phase.*

---

*This formula has a simple familiar form which can be written down from the following elementary kinetic arguments : the random x velocity is $v_e\tilde{B}_x/B$, the mean step size is $(v_e\tilde{B}_x/B)\tau_c$, where τ_c is a correlation time and the associated diffusion rate is $(v_e\tilde{B}_x/B)^2\tau_c$. Taking several modes into account and the fact that the frequency is not zero gives $\kappa \simeq \sum_{k_y} nv_e^2(|\tilde{B}_x(k_y)|^2/B^2)\gamma_k/(\omega_k^2+\gamma_k^2)$. We should note here that in Eq.(12) γ_k is a growth rate and not a damping rate, so application of the elementary kinetic picture is quationable. However, the reconnection process and associated redistribution of heat is a nonsteady transient process in any case and can only be treated as heat conduction in some rough sense. Since the growth can continue for at most a few growth times the kinetic picture probably represents the process as accurately as possible from a heat conduction point of view.

2-2. Electron Heat Conductivity in the Nonlinear Phase

In this section, we assume that only one magnetic island is formed in the system, and consider one Fourier component of k_y. In the nonlinear phase the bounce frequency of the electron motion around the magnetic island, ω_b, becomes larger than $(\omega_k^2+\gamma_k^2)^{1/2}$ for the tearing mode. Consequently the electron heat flux does not continue to transfer along

the perturbed magnetic field. We now estimate the heat conductivity in a heuristic fashion.

We assume the half width of the magnetic island is $W(\tau)$ at the time τ and the electron bounce frequency $\omega_b(\tau)$. Let us pay attention to a single magnetic field line lying on the separatrix. For the electron heat flux on this field line, the step size and the correlation time of heat are thought to be $W(\tau)$ and $\omega_b(\tau)$. After a time interval $\omega_b(\tau)^{-1}$, the electron temperature on this field line will become uniform. The contribution to the heat flux on this field line at the time t may be estimated as,

$$\delta q(t) \simeq W(\tau)^2 \omega_b(\tau) \left[\theta(t-\tau)-\theta(t-\tau-\omega_b^{-1})\right] \frac{\partial T_e}{\partial x} ,$$

where θ is the Heaviside step function. Averaging this quantity over the extent of the magnetic island, the electron heat flux can be estimated as,

$$\begin{aligned} q(t) &\simeq \frac{1}{W_f} \int_0^{W(t)} dw\ \delta q(t) \\ &\simeq \frac{1}{W_f} \int_0^t d\tau\ \frac{dw(\tau)}{d\tau}\ W(\tau)^2\ \delta(t-\tau)\ \frac{\partial T_e}{\partial x} \\ &\simeq \frac{1}{W_f} \frac{dW}{dt} W^2 \frac{\partial T_e}{\partial x} , \end{aligned}$$

where W_f is the saturated width of the magnetic island, and $\delta(t)$ is the delta function. Then we have the electron heat conductivity in the nonlinear phase which is averaged over W_f,

$$\kappa(t) \simeq \frac{1}{W_f} \frac{dW}{dt} W^2 \quad . \tag{16}$$

The above results show that κ is proportional to W^2 if $dW/dt \simeq$ const. in the nonlinear phase.

3. Simulation Model and Results

Particle computer simulations[11] were performed to investigate the tearing instabilities and the consequent heat transport in a low β collisionless plasma. A two-and-one-half dimensional particle model[12] was adopted. In the magnetostatic model, the displacement current is ignored, and hence high frequency modes due to radiation are elminated. For low frequency modes in a low β plasma where tearing takes place, the compressional component of the magnetic field perturbation can be neglected.

The geometry used in the simulation is the same as that shown in Fig.1. The system is periodic in the y direction, and is bounded by two conducting walls located at $x=0$ and $x=L_x$ in the x direction. We assume that there is no spatial variation in the z direction, but particle have three velocity components (v_x, v_y, v_z). The particles which hit the wall are reflected according to the method designated (I) in Ref.(13), which produces neither macroscopic plasma flows nor density perturbations near the walls.

The initial current and temperature profiles used in

the simulations are $J_z(x)=-en_0v_d\exp[-(\ln 2)(x-L_x/2)^2/a^2]$, and $T_{e,i}(x)=1-0.6\tanh[5(x-L_x/2)/L_x]$. Here v_d is the electron drift velocity in the z direction. The initial density is uniform in the system. The initial electron and ion temperature profiles are taken to be the same. 128×128 electrons and ions are followed on a 64×64 spatial grid system. Physical parameters used are $\omega_{ce}/\omega_{pe}=1.5$, $c/v_{te}=5$, $n_0\lambda_D^2=7.8$, $m_i/m_e=16$, $T_e/T_i=1$, $a=5.3$, and $v_{te}=(T_e/m_e)^{1/2}$.

3-1

We first present the results of the simulation excluding longitudinal electric fields for the case of $v_d=0.7v_{te}$. This case is the one discussed in the previous theoretical section. Furthermore with electrostatic effects suppressed the effects on the heat transport of the tearing instability can be separated from those due to convective motion associated with electrostatic fields. This simulation is carried out in such a way that the longitudinal electric field in the equation of motion is neglected without further loss of self-consistency. In this system the linear theory predicts the mode $k_y=\pi/32$ to be unstable.

Figure 2(a) shows the time evolution of the magnetic field lines projected on the x-y plane. The magnetic shear field $B_y(x)$ reverses its direction across the singular surface which lies on the line $x=L_x/2$. The formation of the magnetic island is observed at $\omega_{pe}t\simeq 600$. The island drifts slowly in the direction of the electron diamagnetic

drift until $\omega_{pe}t\simeq 1100$. After $\omega_{pe}t\simeq 1100$ the island stops drifting and turns into a nonlinear pure tearing instability.[14] The width of the magnetic island continues to grow until $\omega_{pe}t\simeq 1700$, at which point it saturates.

The time dependences of the phase and amplitude of the perturbed vector potential $\tilde{A}_z$ are presented in Fig.3(b) and 3(c), respectively. The vector potential is Fourier-analyzed in the y direction and averaged over some range in the x direction ;

$$\tilde{A}_{zn}=\frac{1}{2\Delta L_y}\int_{L_x/2-\Delta}^{L_x/2+\Delta} dx \int_0^{L_y} dy\, A_z \exp(-ik_y y), \qquad (17)$$

$$k_y=2\pi n/L_y \quad .$$

We choose $\Delta=3$ in Figs.3(b) and 3(c). In Fig.3(b) all modes relax to the thermal level during early time ($\omega_{pe}t=0$ to 600). The n=1 mode is unstable in this case, and after $\omega_{pe}t\simeq 600$ the mode grows above the thermal level, whereas the higher n modes continue to fluctuate around the thermal level. During $\omega_{pe}t\simeq 600$ to 1100 the n=1 mode grows with the growth rate of the linear theory as shown by the slope of the solid line in Fig.3(b). This mode saturates at $\omega_{pe}t\simeq 1700$.

The time variation of phase of the n=1 mode is shown in Fig.3(c). The phase varies rapidly with the frequency about ω_{Te}^{*} during the period $\omega_{pe}t\simeq 0$ to 600. After $\omega_{pe}t\simeq 600$, the mode has a frequency of about $0.2\omega_{Te}^{*}$ which agrees with the eigen-frequency predicted by the linear theory. The

frequency of this mode vanishes suddenly at $\omega_{pe}t\simeq1100$, and after this time the frequency remains nearly zero.

In Fig.6(a) we plot the time evolution of the half width of the magnetic island. The growth of the island is almost proportional to time in the nonlinear phase. Figures 2(b) and 2(c) show a time sequence of isothermal lines for the electron parallel and perpendicular internal energy, respectively. Here $nT_{\parallel,\perp}=\langle(v_{\parallel,\perp}-\bar{v}_{\parallel,\perp})^2\rangle$, $\bar{v}_{\parallel,\perp}=\langle v_{\parallel,\perp}\rangle/n$, and $\langle\ \rangle$ represents the ensemble average over the particles around each grid point in the simulation system. The internal energy is higher in the region $x > L_x/2$ than in the $x < L_x/2$ in these figures. The plateau region for the parallel internal energy in Fig.2(b) is observed around the O-point of the magnetic island at $\omega_{pe}t\simeq600$. The gradient of the parallel energy is steep at the X-point. The plateau region spreads as the magnetic island grows. The width of the plateau region is not the same as that of the magnetic island but rather smaller until $\omega_{pe}t\simeq2200$. This indicated the existence of the gradient of the internal energy along magnetic field lines in the island, which is associated with the finite rate at which heat can flow. At $\omega_{pe}t\simeq2200$ the width of the plateau region is equal to that of the island, and the internal energy becomes uniform in the island.

By contrast the plateau region for the perpendicular energy can not be observed at all in the linear phase in Fig.2(c). After $\omega_{pe}t\simeq1100$, the perpendicular energy profile resembles that parallel to the field lines.

To investigate the mechanism of the time variation of the internal energy or the heat transport, we display in Fig.4 the time evolution of the zeroth and the fundamental mode of the electron internal energy on each magnetic field line. Each symbol in Fig.4(a) indicates the average electron internal energy on each magnetic field line. From this figure we see the overall internal energy is not changed so much before the field lines reconnect. At the time the field lines reconnect the internal energy becomes its averaged one on the two field lines, (See, for example, solid circles at $\omega_{pe}t\simeq900$). Of course this is the result of the averaging and not due to the heat transport, since there is a large gradient of energy along this field line. The internal energy on the field lines which do not reconnect until the end is not changed much, but has a tendency to approach the value on the singular surface; this indicates the magnetic field line slips with respect to the internal energy in the inner region.

We illustrate the amplitude of the fundamental mode of the electron internal energy which is defined by $A=(1/L_m)\left|\int dsnT_e" \exp(-i2\pi s/L_m)\right|$ in Fig.4(b). Here L_m is the length of the magnetic field line, and the integration is carried out along a magnetic field line. In the linear phase the reconnection does not occur, but the amplitude grows, nevertheless. The amplitude on the reconnected field line has a peak value at its reconnected time, and after that time the amplitude decays. These results indicate the heat conducts along this field line.

Another remarkable feature which the heat conduction along the field line shows is that there are second peaks due to the amplitude oscillation of the internal energy at $\omega_{pe}t \simeq 2000$.

Let us now examine the heat transport associated with the tearing instabilities more quantitatively. As seen from Figs.2(b) and 2(c) a plateau region in the internal energy is formed within the magnetic island, indicating that there is anomalous electron heat transport across the singular surface. Figure 5(a) shows the time variation of the electron internal energy profile averaged in the y direction. The electron heat conductivity κ for this relaxation of the internal energy is defined by

$$\kappa \frac{\partial T_0}{\partial x} = < (\underset{\sim}{v} - \bar{\underset{\sim}{v}})^2 v_x > \quad . \tag{18}$$

Where T_0 is the initial temperature. As mentioned in Sec.2 the electron heat conductivity associated with the tearing instability is localized within the inner region. We average κ over the inner region ($(1/6)\int_{L_x/2-3}^{L_x/2+3} \kappa \, dx$). Figure 5(b) illustrates the time variation of κ obtained by the above average. κ is normalized to the Bohm diffusion coefficient $n_0 D_B = n_0 T_e/(16 m_e \omega_{ce})$. $\kappa^{(\parallel)}$ and $\kappa^{(\perp)}$ represent the heat conductivity for $(nT_{e\parallel})$ and $(nT_{e\perp})$, respectively. In the linear phase $\kappa^{(\parallel)}$ is a few times as large as $\kappa^{(\perp)}$, which agrees with the prediction of the linear theory. Also in this phase the heat conductivity grows exponentially with time.

At $\omega_{pe}t \simeq 1100$ the growth of the heat conductivity ceases for a while. In the nonlinear phase κ, $\kappa^{(\parallel)}$ and $\kappa^{(\perp)}$ have almose comparable values, and they increase linearly with time. The heat conductivity has its maximum value at $\omega_{pe}t \simeq 1700$, and after that time it decays.

As mentioned in Sec.2 the step size of heat is estimated to be W in the nonlinear phase, which indicates the heat conductivity should be discussed by the value averaged over the saturated width of the magnetic island. Figure 6(b) shows the dependence of the κ averaged over the saturated magnetic island width ($\bar{\kappa} = (1/20)\int_{L_x/2-10}^{L_x/2+10} \kappa \, dx$). Open circles denote the electron heat conductivity obtained by using Eq.(18). Solid circles are obtained by the following method. The relaxation of internal energy is assumed to be described by a diffusion equation,

$$\frac{\partial}{\partial t} nT = \frac{\partial}{\partial x} \kappa \frac{\partial}{\partial x} T_0 \ . \tag{19}$$

Supposing the heat flux is zero at the boundary wall $x=L_x$, κ is obtained from Eq.(19) to be

$$\kappa = \left(\frac{\partial}{\partial t} \int_x^{L_x} dx \, nT \right) / \frac{\partial T_0}{\partial x} \ . \tag{20}$$

The derivative with respect to time is evaluated using a least squares method at intervals of $200\ \omega_{pe}^{-1}$. Solid circles in

Fig.6(b) show the heat conductivity obtained from Eq.(20), which is also averaged over the saturated magnetic island width. Of course it is not obvious that Eq.(19) holds in this case. The term of heat flux, however, dominates other terms in the equation of heat balance[15] in this process, because solid circles have values close to those of the open circles. The linear phase corresponds to the region $W^2 \lesssim 40$ and the nonlinear phase to the region $W^2 \gtrsim 40$ in Fig.6(b). Clearly the electron heat conductivity is proportional to W^4 in the linear phase but to W^2 in the nonlinear phase. The dependence of the computed heat conductivity on the magnetic island width is well explained by the theoretical model presented in Sec.2.

3-2.

In the case of the simulation including the longitudinal electric fields there exists a large heat diffusion even for a thermal plasma. This heat diffusion originates, for example, from the coulomb collisions, the thermally excited high frequency electrostatic waves[16], and convective cells. Thus when these effects are included it becomes more difficult to examine the heat diffusion due to the tearing instability. It can, however, be shown that the electron heat transport is enhanced mainly by the perturbed magnetic field. The longitudinal electric fields are included in the equations of motion by solving the Poisson equation. The tearing instability in this case has a growth rate larger than that

without longitudinal electric fields[14], and the width of the magnetic island grows linearly with time. We have chosen the same physical parameters as those without longitudinal electric fields.

Figure 7 shows the time evolution of the electron heat conductivity for the case of $v_d=0.7v_{te}$. The heat conductivities in Fig.7 are obtained from Eq.(20); we have averaged over the saturated magnetic island width, as was done there. Then the heat conductivity includes effectively the viscosity term and so on in the equation of heat balance[15]. Comparing this heat conductivity with that obtained from Eq.(18) the difference between these is smaller than twenty percents. In Fig.7 the response of $\kappa^{(\parallel)}$, $\kappa^{(\perp)}$ and κ to the tearing instability is very similar.

The dependence of the electron heat conductivity on W^2 is shown in Fig.8(a). In the case of the simulation including the longitudinal electric fields the heat conductivity seems to be always proportional to W^2. Another feature for these cases is that the heat conductivity approaches a finite value in the limit of W=0, which is about $0.15n_0D_B$. This heat conductivity is associated with thermal electrostatic fluctuations because this level of heat conductivity exists even in the simulation excluding the magnetic fluctuations. This initial level of transport probably marks the early transport proportional to W^4 which is seen in the earlier calculations without the electrostatic fields. The fact that the initial transport is larger than that observed during the

W^4 phase of Fig.6(b) strongly indicates this.

Figure 8(b) shows the dependence of ($d\kappa/dW^2$) on (dW/dt) which is observed in the above simulations. The solid line has a slope $d(\kappa/n_0 D_B)/dW^2=0.2dW/d(\omega_{pe}t)$. The observed quantities denoted by solid circles agree well with the solid line. Thus we conclude the electron heat conductivity associated with the tearing instability has the relation $\kappa \propto (dW/dt)W^2/W_f$ at least in the nonlinear phase.

4. Conclusions and Discussions

We have presented the behavior of the collisionless tearing instabilities in a plasma with non-uniform temperature. The anomalous electron heat transport associated with these modes was investigated using a two-and-one-half dimensional magnetostatic particle simulation code. We derived the linear growth rates and frequencies of the tearing instabilities numerically. We found that the tearing instability has a tendency to be stabilized by a plasma temperature gradient. The tearing instability appears to grow less strongly for a non-uniform plasma temperature even when the system is unstable to tearing. It is observed that the tearing instability propagates in the direction of the electron diamagnetic drift with a frequency of about $\omega \simeq 0.2\omega^*_{Te}$. This drift tearing instability saturates at a low amplitude and turns into a nonlinear pure tearing instability. In this nonlinear phase the width of the magnetic island grows linearly with time.

We have demonstrated that the electron heat transport

associated with the tearing instability is enhanced mainly by the perturbed magnetic field in the temperature gradient direction. The electron internal energy on a magnetic field line is found to change suddenly the reconnection with another field line takes place. Further amplitude oscillations of the internal energy are observed within the magnetic island. A plateau region for the electron internal energy is formed inside the magnetic island. The electron heat conductivity originating from the heat flux across the singular surface is proportional to W^4 in the linear phase, while it is proportional to $(dW/dt)W^2$ in the nonlinear phase. In particular the electron heat conductivity for $(nT_{e\parallel})$ has a value about a few times as large as that for $(nT_{e\perp})$ in the linear phase. On the other hand both heat conductivity have comparable values in the nonlinear phase. In the case of the simulation including the longitudinal electric fields we fail to observe the W^4 dependence of the electron heat conductivity. The reason for this is hypothesized to be the heat transport associated with the tearing instability is hidden behind the large background heat transport existing in the plasma due to the electrostatic fluctuations.

We have not mentioned the ion heat transport so far. The maximum value of the ion heat conductivity ($\simeq 0.2n_0D_B$) was observed to be at most one-fourth as large as that of the electron heat conductivity although the ion heat flux was also enhanced by the tearing instability. In this case the

electron heat should transport keeping the charge neutrality. We failed to observe the clear formation of the ambipolar potential along the magnetic field lines. However, the electron heat conductivity was observed to be suppressed by the longitudinal electric fields, because the electron heat conductivity had the relation $\kappa/n_0 D_B \simeq 0.2 W^2 dW/d(\omega_{pe} t)$ in the simulation with electrostatic fields (see Fig.8) but $\kappa/n_0 D_B \simeq 0.35 W^2 dW/d(\omega_{pe} t)$ in the nonlinear phase of the simulation without electrostatic fields (see Fig.6).

Acknowledgements

The author gratefully acknowledges Professor T. Kamimura for his useful discussions and encouragements. He is also grateful to Professor Y. Terashima and Professor J.M. Dawson for their valuable discussions and critical reading of this manuscript. He wishes to thank Professor J.D. Callen for his helpful discussions and to the members of the computer center of the Institute of Plasma Physics, Nagoya University, for their assistance with the computer simulations.

References

1) S. Von Coeler, W. Stodiek and N. Sauthoff: Phys. Rev. Lett. 33 (1974)1201.

2) R.D. Hazeltine and H.R. Strauss: Phys. Rev. Lett. 37 (1976)102.

3) T.H. Stix: Nucl. Fusion 18 (1978)353.

4) A.B. Rechester and M.N. Rosenbluth: Phys. Rev. Lett. 40 (1978)38.

5) J.F. Drake and Y.C. Lee: Phys. Fluids 20 (1977)1341.

6) J.F. Drake and Y.C. Lee: Phys. Rev. Lett. 39 (1977)453.

7) R.D. Hazeltine, D. Dobrott and T.S. Wang: Phys. Fluids 18 (1975)1778.
R.D. Hazeltine and H.R. Strauss: Phys. Fluids 21 (1978)1007.
S.M. Mahajan, R.D. Hazeltine, H.R. Strauss and D.W. Ross: Phys. Fluids 22 (1979) 2147.

8) S.M. Mahajan, R.D. Hazeltine, H.R. Strauss and D.W. Ross: Phys. Rev. Lett. 41 (1978)1375.

9) A.A. Galeev: Phys. Fluids 21 (1978)1353.

10) B.D. Fried and S.D. Conte: The Plasma Dispersion Function (Academic Press, New York 1961).

11) A.B. Langdon and C.K. Birdsall: Phys. Fluids 13 (1970)2115.
W.L. Kruer, J.M. Dawson and B. Rosen: J. Comp. Phys. 13 (1973)114.

12) C.W. Nielson and H.R. Lewis: Methods in Computational Physics (Academic Press, New York, 1976, Vol.16, P.367).
J. Busnardo-Neto, P.L. Pritchett, A.T. Lin and J.M. Dawson: J. Comp. Phys. 23 (1977)300.

13) H. Naitou, S. Tokuda and T. Kamimura: J. Comp. phys. 33 (1979) 86.

14) I. Katanuma and T. Kamimura: Res. Note of Inst. Plasma Physics (Nagoya), IPPJ 370 (January 1979), (Phys. Fluids to be published).

15) S.I. Branginskii: Transport Processes in a Plasma, edited by M.A. Leontovich (Consultants Bureau, New York 1970).

16) H. Naitou: J. Phys. Soc. Jpn. 48 (1980) 608.

Figure Caption

Fig.1. Initial temperature and current profiles shown in the slab geometry bounded by conducting walls in the x direction. The current flows in the z direction producing a sheared magnetic field $|B_s| << |B_0|$.

Fig.2. Time variation of the magnetic field lines (a), and the isotherms for $nT_{e"}$ (b) and $nT_{e\perp}$ (c) projected on the x-y plane.

Fig.3(a). Linear dispersion relation of the tearing instability for the case $k_y=\pi/32$. Open circles corresponds to the parameters of the simulation.

Fig.3(b). Time evolution of phase of the perturbed vector potential $\tilde{A}_z(k_y=\pi/32)$. $\tilde{A}_z$ is averaged over the width 6 around $x=L_x/2$. The slope of the solid line has the frequency obtained from linear theory.

Fig.3(c). Time evolution of amplitude of $\tilde{A}_z(k_y=n\pi/32)$. The slope of the solid line corresponds to the linear growth rate.

Fig.4. Time variation of the average electron energy ($nT_{e"}$) on a magnetic field line. The integration is along a magnetic field line. Symbols of the same type denote the quantity on the magnetic field lines which have the same value of $|A_z|$.

4(a). Time variation of the average electron energy parallel to the magnetic field line.

4(b). Time variation of the fundamental Fourier component of the parallel electron energy along magnetic field lines.

Fig.5(a). Time variation of the electron energy profiles averaged in the y direction.

Fig.5(b). Time variation of the electron heat conductivity which is normalized by $n_0 D_B = n_0 T_e/(16 m_e \omega_{ce})$.

Fig.6(a). Time evolution of the half width of the magnetic island.

Fig.6(b). The dependence of the electron heat conductivity on W.

Fig.7. Time variation of the electron heat conductivity.

Fig.8(a). The dependence of the electron heat conductivity on W. Each symbol represents the results obtained from the simulations for different parameter v_d.

Fig.8(b). The dependence of A on B. A represents $d(10\kappa/n_0 D_B)/dW^2$. B means $dW/d(\omega_{pe} t)$.

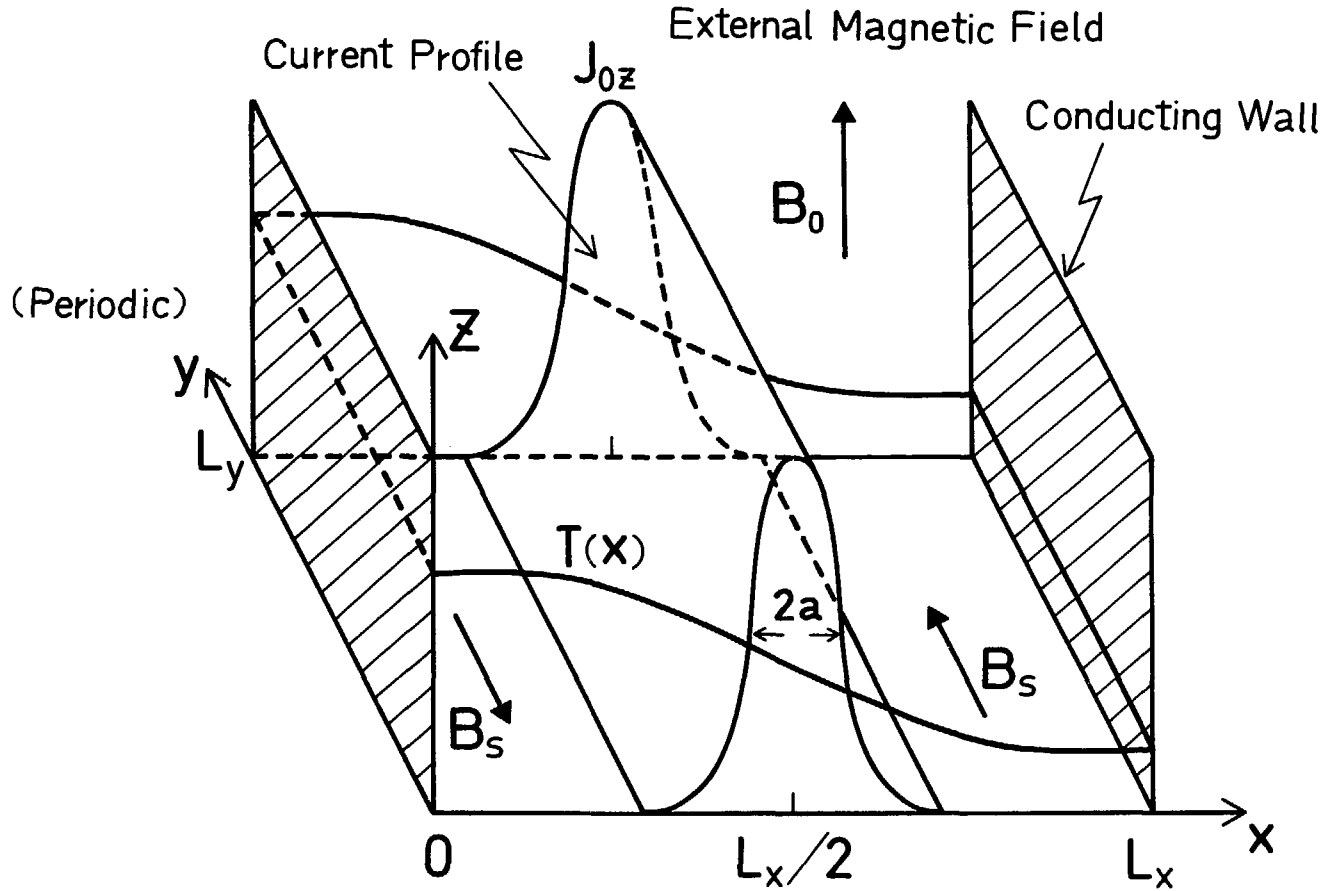
External Magnetic Field
Current Profile
J_{0z}
Conducting Wall
B_0
(Periodic)
z
y
L_y
T(x)
2a
B_s
B_s
0
$L_x/2$
L_x
x

Fig.1

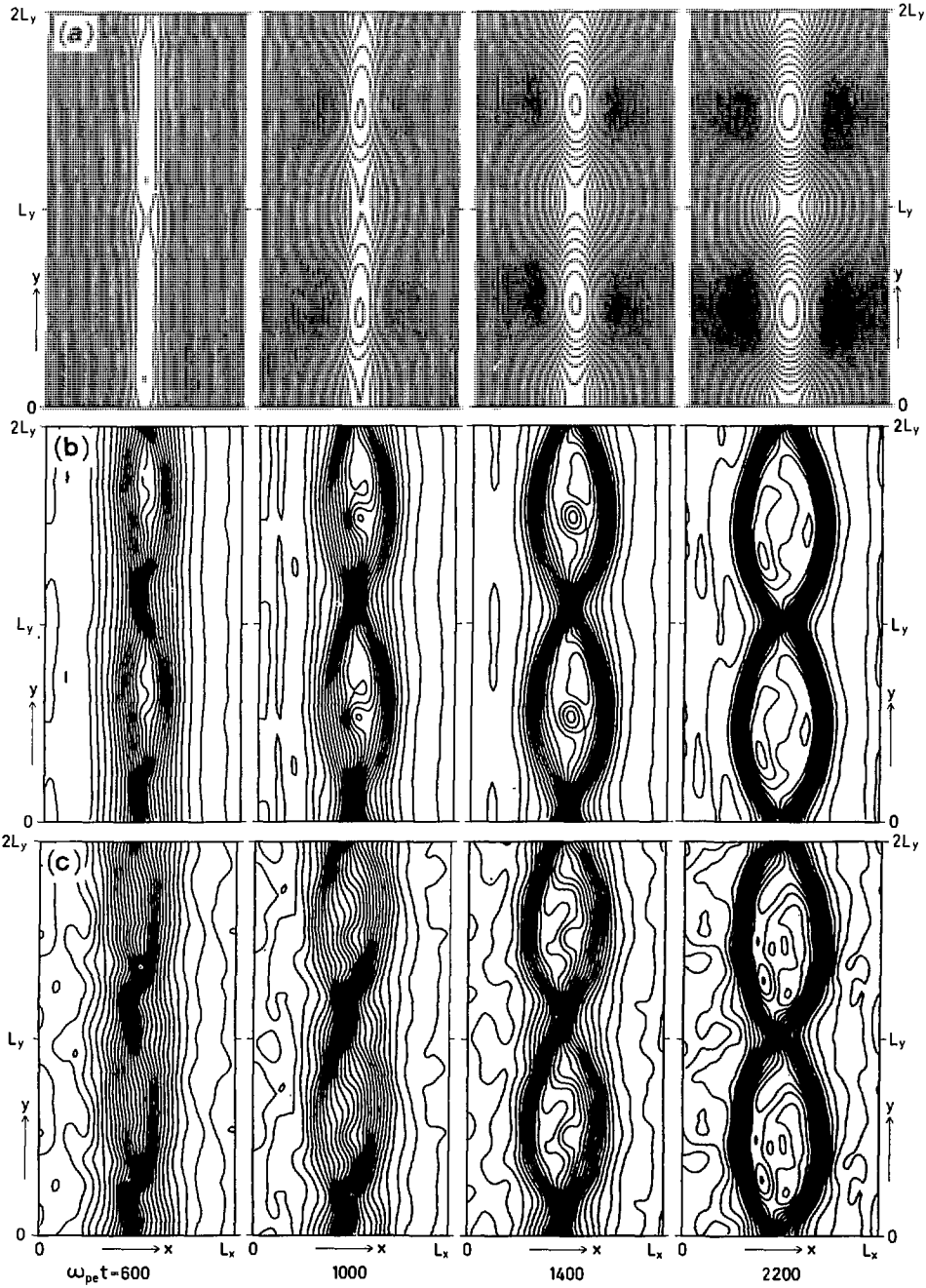

Fig.2

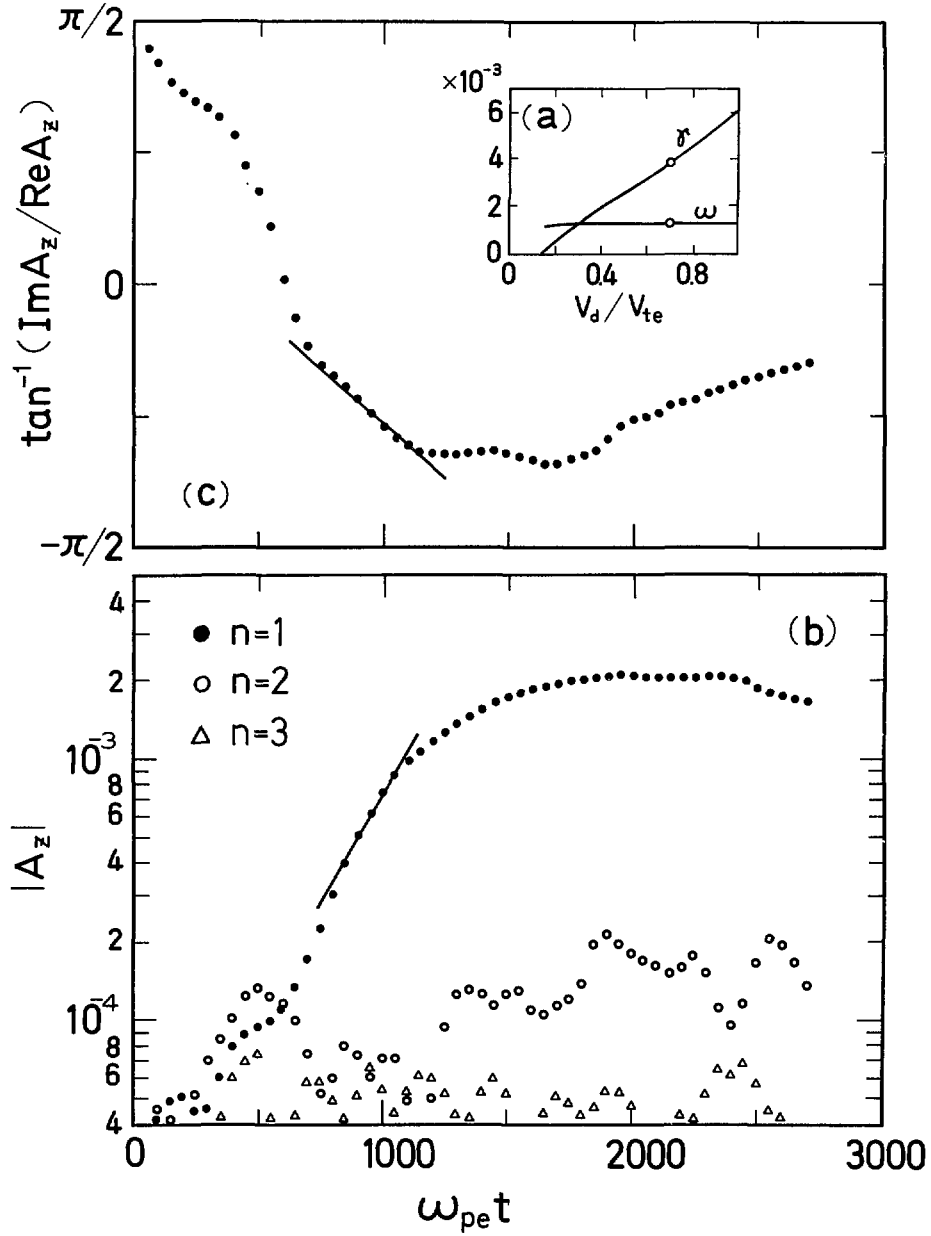
π/2
0
-π/2
tan⁻¹(ImAz/ReAz)
(c)
×10⁻³
6
4
2
0
(a)
γ
ω
0
0.4
0.8
Vd/Vte
4
2
10⁻³
8
6
4
2
10⁻⁴
8
6
4
|Az|
● n=1
○ n=2
△ n=3
(b)
0
1000
2000
3000
ωpet

Fig.3

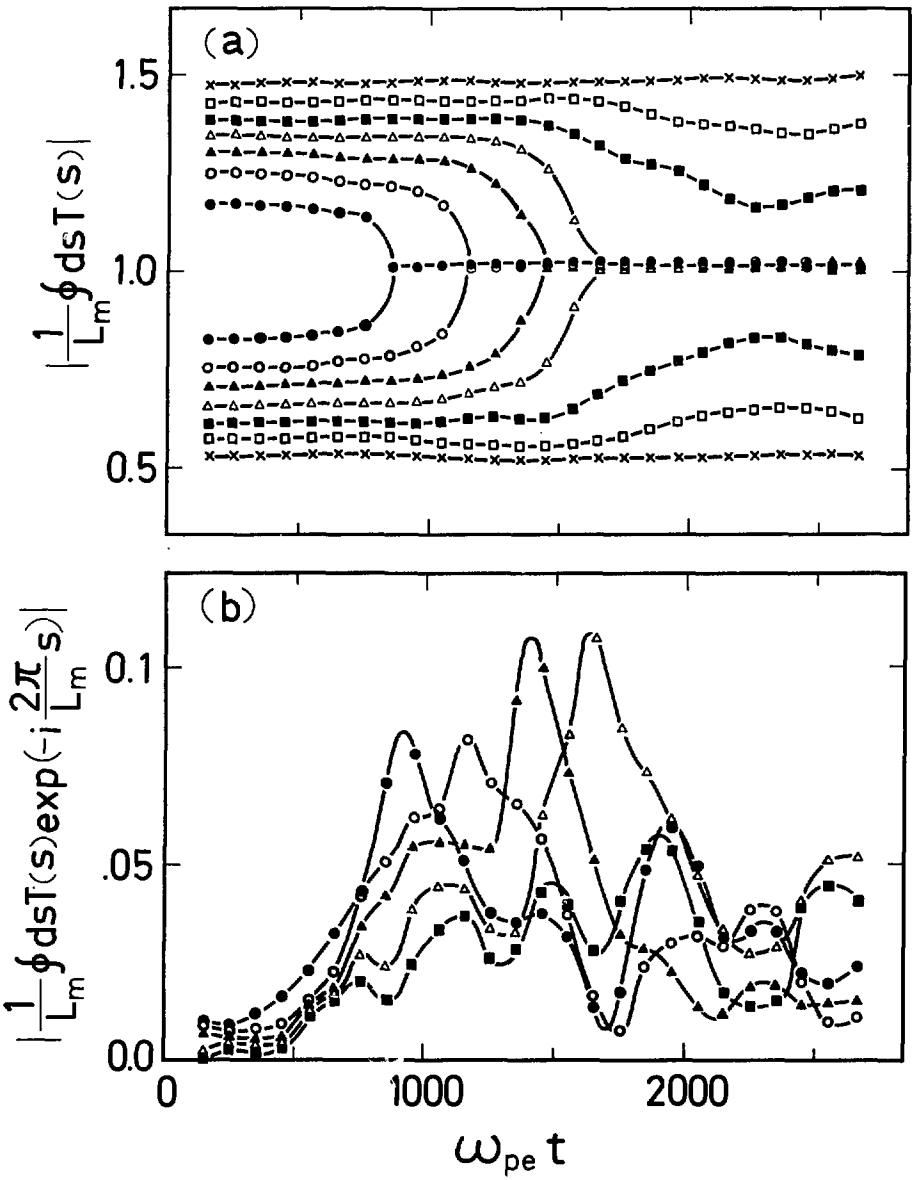
(a)
1.5
1.0
0.5
$|\frac{1}{L_m}\oint ds T(s)|$
(b)
0.1
.05
0.0
$|\frac{1}{L_m}\oint ds T(s) \exp(-i\frac{2\pi}{L_m}s)|$
0
1000
2000
$\omega_{pe}\, t$

Fig.4

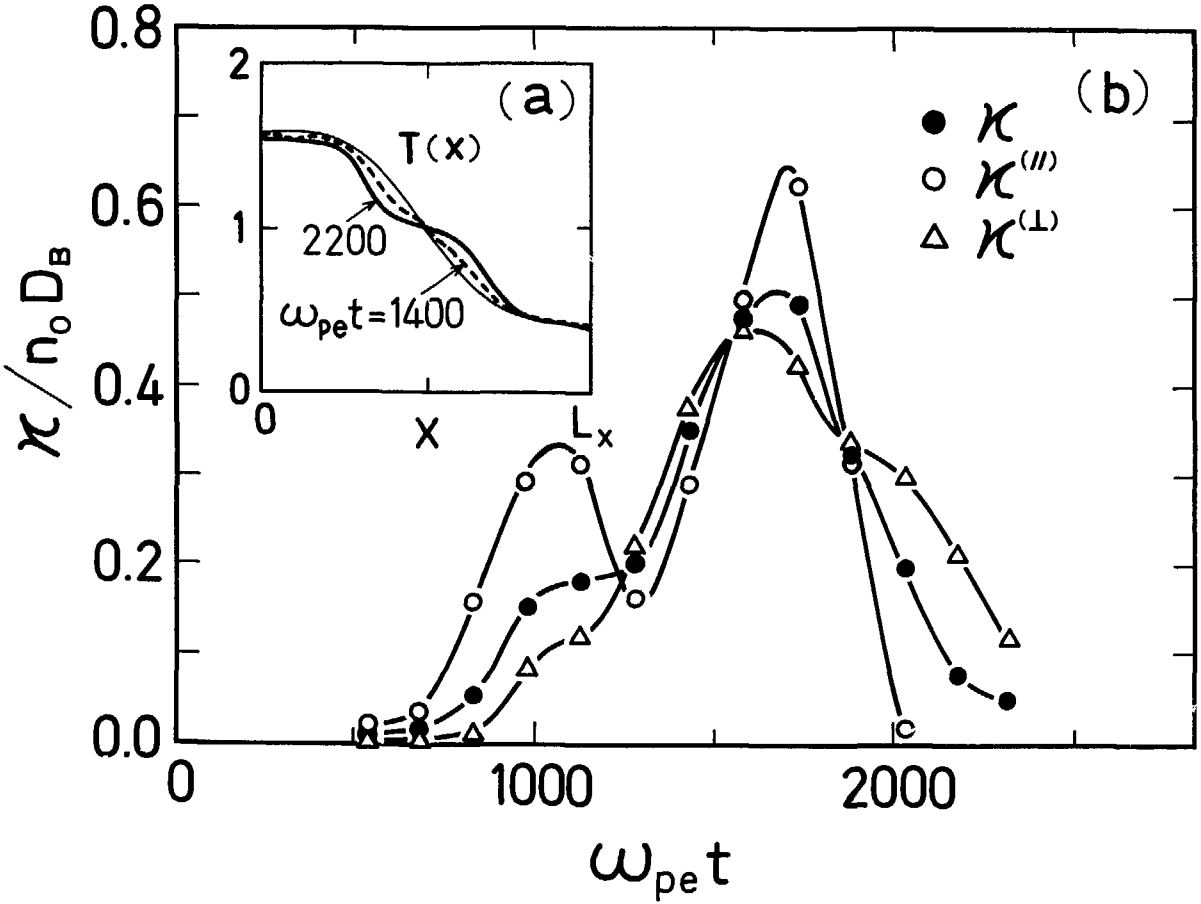
0.8
0.6
0.4
0.2
0.0
0
1000
2000
$\kappa/n_0 D_B$
$\omega_{pe}t$
(a)
T(x)
2200
$\omega_{pe}t$=1400
2
1
0
0
X
L_x
(b)
κ
$\kappa^{(//)}$
$\kappa^{(\perp)}$
c

Fig.5

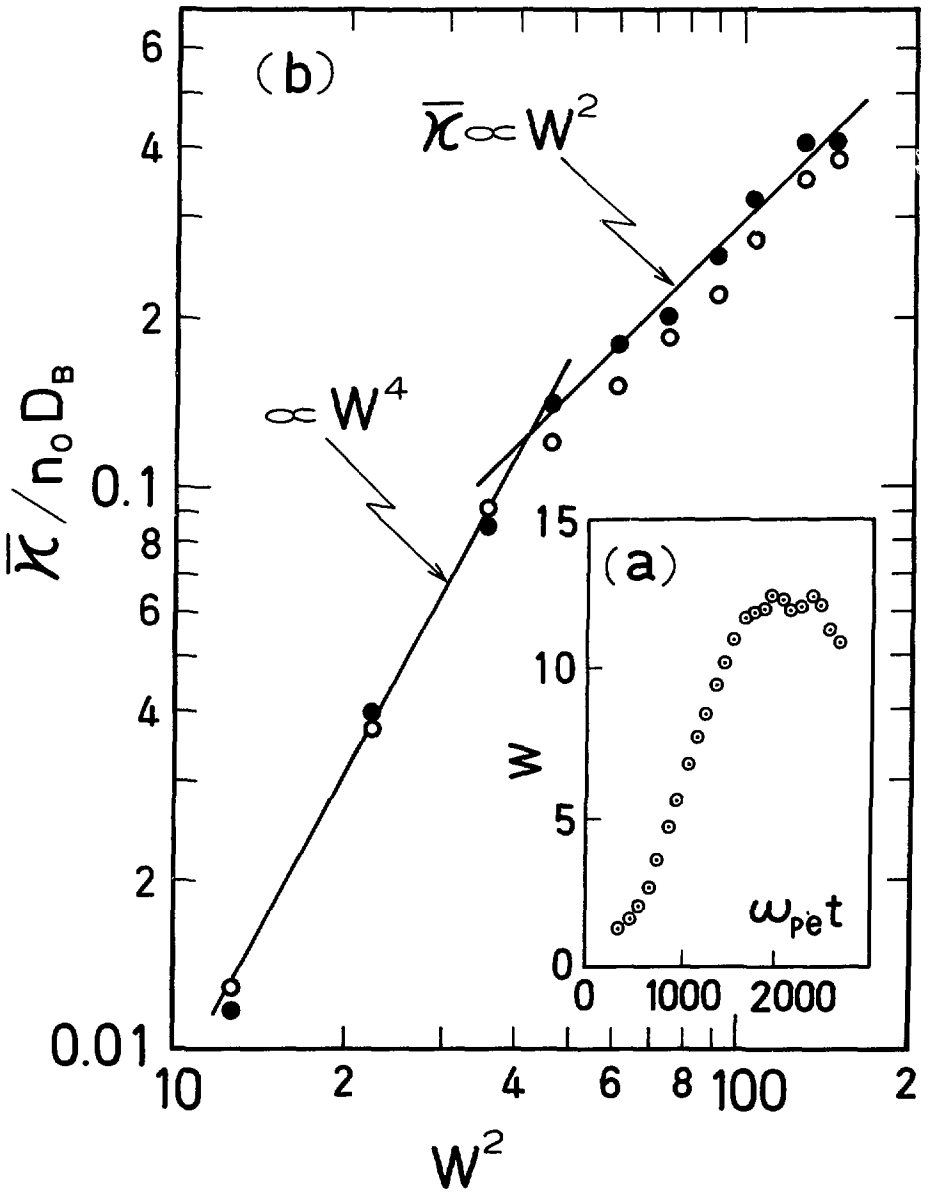
(b)
$\bar{\kappa} \propto W^2$
$\propto W^4$
$\bar{\kappa}/n_0 D_B$
W^2
6
4
2
0.1
8
6
4
2
0.01
10
2
4
6
8
100
2
(a)
W
15
10
5
0
0
1000
2000
$\omega_{pe}t$

Fig.6

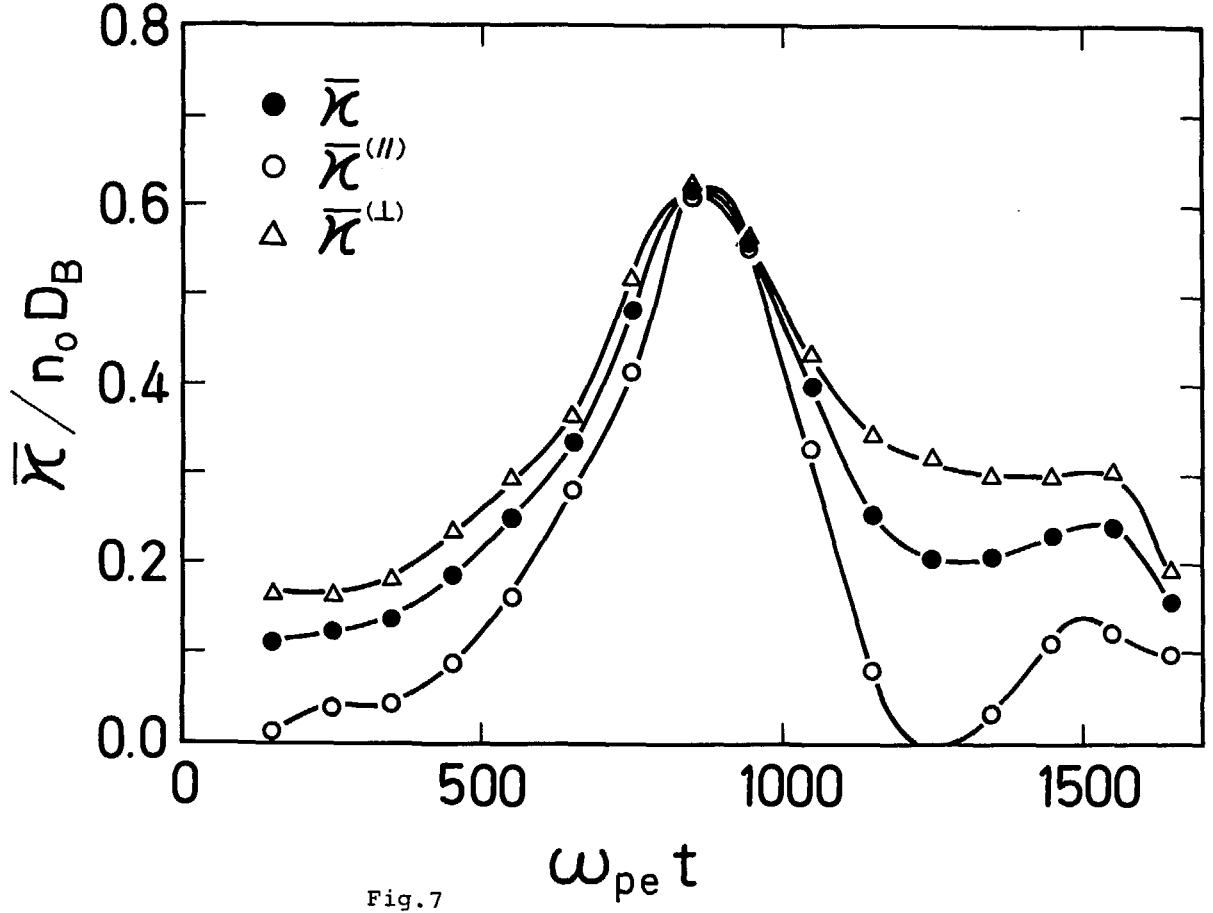
0.8
0.6
0.4
0.2
0.0
0
500
1000
1500
$\bar{\kappa}$
$\bar{\kappa}^{(//)}$
$\bar{\kappa}^{(\perp)}$
$\bar{\kappa} / n_0 D_B$
$\omega_{pe} t$

Fig.7

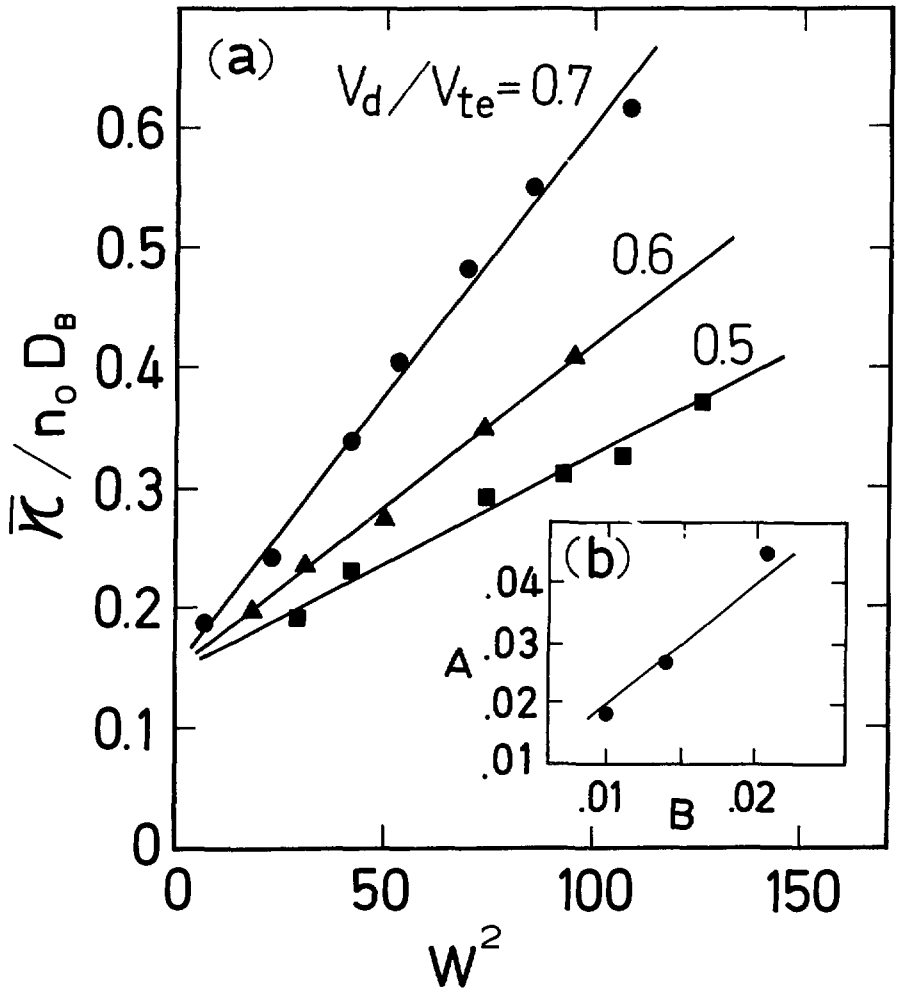
(a)
V_d/V_{te}=0.7
0.6
0.5
$\bar{\kappa}/n_0 D_B$
0.4
0.3
0.2
0.1
0
0.6
0.5
(b)
.04
.03
A
.02
.01
.01
B
.02
0
50
100
150
W^2

Fig.8